



Understanding the enzyme–ligand complex: insights from all-atom simulations of butyrylcholinesterase inhibition

Walter Alvarado^{a*}, Parker Ladd Bremer^{b*}, Angela Choy^c, Helen N. Dinh^b, Aingty Eung^d, Jeannette Gonzalez^e, Phillippe Ly^b, Trina Tran^b, Kensaku Nakayama^b, Jason P. Schwans^b and Eric J. Sorin^b

^aDepartment of Physics & Astronomy, California State University Long Beach, Long Beach, CA, USA; ^bDepartment of Chemistry & Biochemistry, California State University Long Beach, Long Beach, CA, USA; ^cDepartment of Chemical Engineering, California State University Long Beach, Long Beach, CA, USA; ^dDepartment of Computer Engineering & Computer Science, California State University Long Beach, Long Beach, CA, USA; ^eDepartment of Biological Sciences, California State University Long Beach, Long Beach, CA, USA

Communicated by Ramaswamy H. Sarma

ABSTRACT

All-atom molecular dynamics simulations of butyrylcholinesterase (BChE) *sans* inhibitor and in complex with each of 15 dialkyl phenyl phosphate derivatives were conducted to characterize inhibitor binding modes and strengths. Each system was sampled on the 250 ns timescale in explicit ionic solvent, for a total of over 4 μ s of simulation time. A K-means algorithm was used to cluster the resulting structures into distinct binding modes, which were further characterized based on atomic-level contacts between inhibitor chemical groups and active site residues. Comparison of experimentally observed inhibition constants (K_i) with the resulting contact tables provides structural explanations for relative binding coefficients and highlights several notable interaction motifs. These include ubiquitous contact between glycines in the oxyanion hole and the inhibitor phosphate group; a sterically driven binding preference for positional isomers that extend aromaticity; a stereochemical binding preference for choline-containing inhibitors, which mimic natural BChE substrates; and the mechanically induced opening of the omega loop region to fully expose the active site gorge in the presence of choline-containing inhibitors. Taken together, these observations can greatly inform future design of BChE inhibitors, and the approach reported herein is generalizable to other enzyme–inhibitor systems and similar complexes that depend on non-covalent molecular recognition.

ARTICLE HISTORY

Received 30 November 2018
Accepted 6 March 2019

KEYWORDS

Organophosphate; reversible inhibition; contact table; omega loop; docking

1. Introduction

Alzheimer's disease, Parkinson's disease and preeclampsia are all associated with overactivity of butyrylcholinesterase or BChE (Darvesh, Hopkins, & Geula, 2003; Dong et al., 2017; Giacobini, 2001; Greig et al., 2005; Mesulam et al., 2002; Rahimi et al., 2013), a non-specific enzyme that hydrolyzes the neurotransmitter acetylcholine and other choline-based esters (Allderdice et al., 1991). Because these health problems continue to afflict the population, the development of selective and potent BChE inhibitors continues to be a valuable area of research (Akıncioğlu et al., 2017; Cavallaro, Moglie, Murray, & Radivoy, 2018; Giacobini, 2004; Kamal et al., 2008; Senol et al., 2017; Yu et al., 2017). Organophosphorous compounds constitute one class of inhibitors that have been explored thus far (Fukuto & Metcalf, 1956; Hong & Raushel, 1999; Moretto, 1998). Structurally, they are related to metrifonate, an irreversible inhibitor of acetylcholinesterase, or AChE, shown to increase cognitive ability in patients suffering from Alzheimer's disease (Farlow & Cyrus, 2000).

We previously explored the inhibitory potential of dialkyl phenyl phosphates (DAPs) and, based on the success of that initial study (Law et al., 2007), we opted to systematically synthesize, assay and model derivatives of the dibutyl phenyl

phosphate species (Nakayama et al., 2017). This report builds on that previous effort by exploring the binding mechanics of DAP derivatives through all-atom, explicit solvent, molecular dynamics (MD) simulations. Indeed, this proof-of-concept effort presents an approach to understanding and exploring the binding mode space of molecular complexes via rigorous MD simulations and a novel binding mode analysis based on high-dimensionality clustering and visualization of interactions between chemical groups in each inhibitor and the residues that compose the BChE active site gorge.

This gorge, or pocket, is approximately 690 Å³ in volume (Pezzemanti, Nachon, & Chatonnet, 2011) and, as represented in Figure 1, contains a number of subsites that play various roles during catalysis. Substrates approaching BChE first interact with residues in the peripheral anionic site, or PAS (Masson, Froment, Bartels, & Lockridge, 1996; Masson et al., 1997), which passes the substrate further into the gorge (Chatonnet & Lockridge, 1989; Masson et al., 1996, 1997; Nicolet, Lockridge, Masson, Fontecilla-Camps, & Nachon, 2003), where the acyl binding site, or ABS (Dighe et al., 2016; Pezzemanti et al., 2011; Wandhammer et al., 2011), and the choline binding site, or CBS (Biberoglu, Tacal, & Akbulut, 2011; Dighe et al., 2016; Pezzemanti et al., 2011), assist in

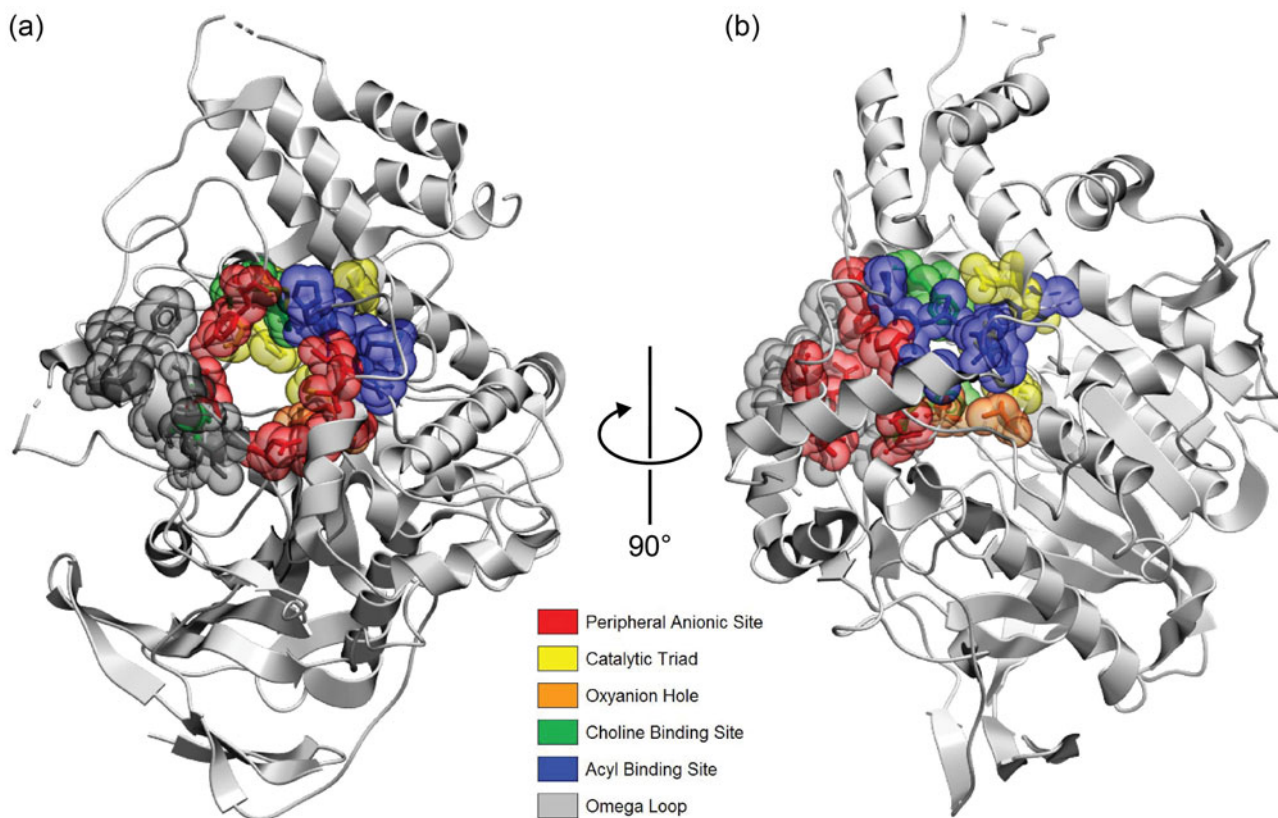


Figure 1. Visualization of BChE in grayscale ribbon mode with active site residues shown as semi-transparent van der Waals surfaces and colored according to the inset color key, as described in the text, (a) facing into the active site gorge and (b) rotated 90° about the vertical axis.

the positioning of the substrate for catalysis. At the bottom of the gorge lies the catalytic triad, or CAT (Chiou, Huang, Hwang, & Lin, 2009; Zhan & Gao, 2005), and the oxyanion hole, or OAH (Warshel, Naray-Szabo, Sussman, & Hwang, 1989; Zhan & Gao, 2005). The CAT of BChE operates similarly to the Ser–His–Asp motif seen in many serine proteases, with the aspartic acid residue replaced by glutamic acid (Warshel et al., 1989). During catalysis, the OAH stabilizes high-energy anionic intermediates and transition states via hydrogen bonding. Additionally, the omega loop, or OML (Fetrow, 1995; Masson, Xie, Froment, & Lockridge, 2001), resides near the binding pocket entrance and can, depending on the interactions of the inhibitor with active site gorge residues, seal off the gorge via a capping mechanism or, as we explore later, shift to fully expose the pocket in the presence of certain choline-containing inhibitors that were initially proposed in an effort to mimic natural substrates.

2. Methods

A model of human BChE was prepared by removing all water molecules, ions and ligands from the crystal structure (PDB ID: 1P0I), inserting missing atoms and side chains (none of which were near to, or part of, the enzyme active site gorge) and performing geometry optimization on these regions using Accelrys Discovery Studio (BIOVIA, 2007). The resulting structure was then energy minimized, including side-chain rotamer relaxation, using the SwissPDB software (Guex & Peitsch, 1997). Simulated inhibitor molecules were modeled

using the general AMBER force field (Wang, Wolf, Caldwell, Kollman, & Case, 2004), which was designed in tandem with partial charge calculation via the semi-empirical (AM1) method with bond charge correction (BCC) to match the molecular electrostatic potential computed at the Hartree–Fock 6-31G* theory level (Jakalian, Bush, Jack, & Bayly, 2000; Jakalian, Jack, & Bayly, 2002). Partial charges were calculated using the Quacpac Tool Kit from OpenEye Scientific (Ellingson et al., 2014).

All-atom MD simulations of native BChE *sans* inhibitor, and of the protein in complex with each inhibitor described below, were performed using GROMACS 4.5.3 software suite (Pronk et al., 2013). The protein and counterions were modeled using the AMBER03 force field (Duan et al., 2003) ported to the GROMACS suite (Sorin & Pande, 2005) and solvated with the TIP3P explicit water model (Mahoney & Jorgensen, 2000). To optimize simulation time, a periodic octahedral box was used, yielding a total system size of approximately 72,350 atoms. All simulations were performed in the NPT ensemble at 1.0 atm and 300 K using the Berendsen and modified-Berendsen barostat and thermostat, respectively (Berendsen, Postma, van Gunsteren, DiNola, & Haak, 1984; Bussi, Donadio, & Parrinello, 2007), with a 2.0 fs time step using the LINCS algorithm (Hess, Bekker, Berendsen, & Fraaije, 1997) to constrain bonds involving hydrogen atoms. A switching function from 7 to 9 Å and a standard long-range correction term were applied to van der Waals interactions, and electrostatic interactions beyond 9 Å employed a reaction-field treatment with a dielectric coefficient of 80.

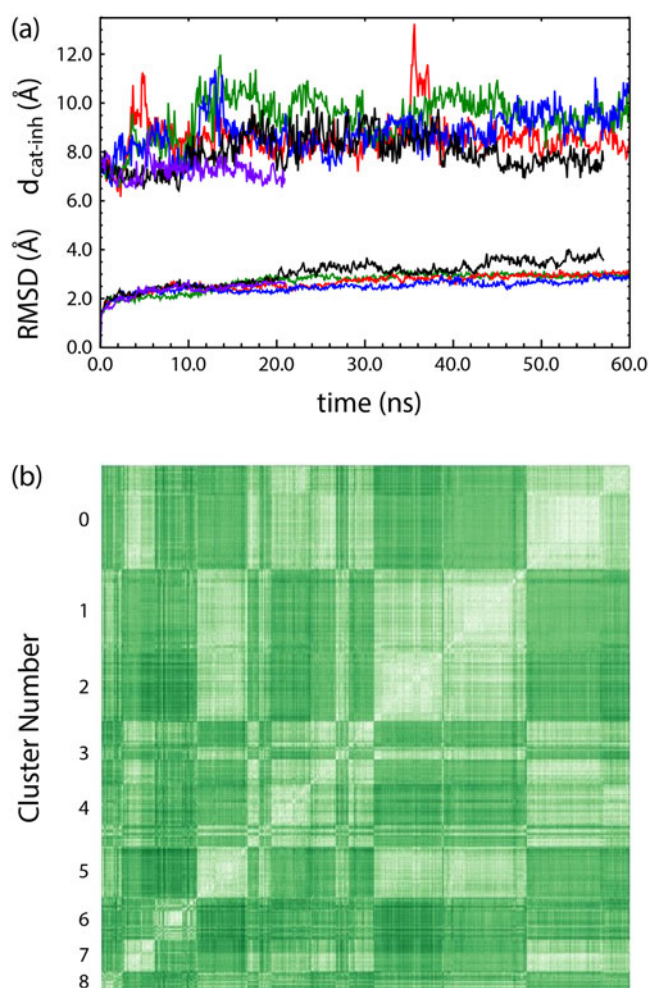


Figure 2. (a) All-atom RMSD of BChE (bottom) and absolute distance between the catalytic triad center-of-mass and inhibitor center-of-mass (top) for the first 60.0 ns of DAP4 simulations. (b) Similarity matrix for DAP4, which shows the root-mean-squared difference between descriptor vectors between and within each cluster of the DAP4 sampling, where lighter and darker shades represent higher and lower similarities, respectively. The matrix is sorted from most populated cluster 0 to least populated cluster 8.

The ICM Pro computational suite (Abagyan, Totrov, & Kuznetsov, 1994; An, Totrov, & Abagyan, 2005) was used to perform 10,000 molecular docking trials of each inhibitor within the active site gorge of BChE, where the best scoring docked structure was taken as the MD starting conformation for each inhibitor. Five simulations per BChE–inhibitor complex were then collected, with an average simulation time of approximately 60 ns, thereby yielding 4.23 μ s of total sampling with structures stored every 100 ps with the initial 10.0 ns equilibration period of each simulation excluded from the analysis reported below. While this is an appreciable timescale on which to simulate systems of this size in atomistic detail, it is important to emphasize that the limited sampling per complex reported herein is not expected to have reached, or to provide information regarding, conformational equilibrium or statistically relevant populations of the observed binding modes. For this reason, the characterization below focuses on the qualitative nature of protein–inhibitor binding.

Following 3D alignment of each resulting complex structure to a reference protein structure, each conformation was

characterized by the position of the inhibitor relative to the protein center-of-mass and vectors internal to the inhibitor representing the orientation of the three constituents bonded to the phosphate group, as well as a vector normal to the aromatic group to capture rotational position. These vector components were then used to cluster inhibitor conformations into thermodynamic microstates, or binding poses. To address the primary limitation present in most K-means algorithms, the need to know *a priori* how many data clusters are present in a given data set (Shao, Tanner, Thompson, & Cheatham, 2007), a modified K-means algorithm that initially overestimates the number of clusters present in the data and then slowly eliminates empty clusters (Sorin & Pande, 2005) was employed. The most statistically dominant binding poses were then characterized in terms of specific interactions between chemical groups within the inhibitor and the binding pocket residues of the enzyme. Atomic interactions for each binding mode were identified as protein atoms within 5.0 Å of inhibitor phosphate or aromatic group atoms, or within 3.0 Å of alkyl or choline group atoms, which occurred with a frequency of 0.25 or higher.

3. Results and discussion

3.1. Reference inhibitor and contact tables

As the largest of the DAPs that did not encounter solubility issues during assay in our recent collaborative study (Nakayama et al., 2017), dibutyl phenyl phosphate (DAP4) serves as the reference structure to which the inhibitors studied herein are compared. This moiety has a measured K_i value of 94.5(\pm 9.0) μ M and an optimal ICM Pro docking score of -82.6 . A total MD simulation time of 268.9 ns was collected over five simulations for DAP4. To assess the stability of our simulated complexes, the all-atom root-mean-square deviation (RMSD) of the protein was monitored in tandem with the distance between the center-of-mass of the catalytic triad and the inhibitor center-of-mass, which are shown in Figure 2(a) for the BChE–DAP4 reference complex. While the inhibitor is quite dynamic with respect to the catalytic triad location, the protein RMSD remains below 3.25 Å in all but one simulation, during which a maximum protein RMSD of 4.04 Å was observed.

The clustering of structures from our DAP4 simulations yielded nine statistically relevant binding poses. To assess the quality of this clustering result, we defined the similarity score for any two structures as the root-mean-squared difference between the min–max normalized clustering vectors for those structures, where highly similar inhibitor structures would thus yield low numeric scores. Figure 2(b) shows the resulting similarity matrix for our DAP4 clustering. As expected, intra-cluster similarities along the diagonal are generally very good, and off-diagonal comparisons demonstrate far lower inter-cluster similarity. Given our focus on small molecules in non-covalent complex with a large protein, it is not unexpected to see some similarity between a limited number of cluster pairs, as multiple clusters can include a significant number of shared protein–inhibitor interactions. This does not imply, however, that the

Waals contact between an alkyl chain and SER287, as well as added non-polar interactions between an alkyl group and numerous hydrophobic side chains in the omega loop region.

3.3. Di- and trimethylphenyl derivatives

Additional methylations of the phenyl ring led to the di- and trimethylphenyl derivatives of MET3 and MET4 assayed recently (Nakayama et al., 2017) and shown in Table 4. While the addition of second and third methyl groups to the meta positions of MET4 had no appreciable impact on inhibitor strength, the di-*m*-methyl species (DIM5) shown in Table 4 improved the measured K_i value by an additional order of magnitude.

As illustrated in Table 5, this group of inhibitors maintained significant alkyl chain contact with acyl binding site and catalytic triad residues, as well as phosphate and alkyl chain contacts with residues in the oxyanion hole, and π -stacking interactions between the phenyl group and TRP82 in the CBS, all of which were observed for DAP4 and the methylphenyl series above. That we observed consistent binding motifs for these multi-methylated species and the previously discussed inhibitors justifies the relative constancy of measured K_i values for both DIM4 and TRIM shown in Table 4. In contrast to DAP4 and the MET series, the methylated phenyl group of both DIM4 and TRIM also showed significant π -stacking with TRP430, electrostatic interaction with MET437 and van der Waals contact with TYR440, all of which are shown in the APR section of Table 5.

The most potent inhibitor examined in this study, DIM5, exhibits an improved K_i value that is an order of magnitude lower than the MET4, DIM4 and TRIM analogs. This is largely due to the positioning of the DIM5 phosphate group, which forms hydrogen bonds with catalytic triad residues SER198 and HIS438, something that is seen only sparingly for the previously discussed inhibitors above. It is notable that this PO_4 -CAT hydrogen bonding is analogous to the first step in the BChE catalytic mechanism of natural substrate hydrolysis (Sirin & Zhang, 2014) and stabilizes the deep-pocket positioning of DIM5. In addition, the DIM5 phosphate group interacts not only with the GLY residues in the oxyanion hole, GLY116 and GLY117, but also with the neighboring GLY115, thereby strengthening the anchoring of the phosphate group to the protein backbone in the CAT region.

It is also noteworthy that, of the three di- and trimethylphenyl species, only DIM5 consistently maintains interaction between the inhibitor aromatic group and both GLN119 (PAS) and THR120 (APR), which were observed for DAP4 and MET series inhibitors. The capacity of GLN119 and THR120 to interact with all three types of functional groups present in the studied inhibitors reflects the amphipathic nature of these amino acids, which allows them to adopt hydrophobic and hydrophilic roles. That the versatility of these residues allows them to interact with chemically disparate functional groups suggests that these interactions are sterically driven and will persist

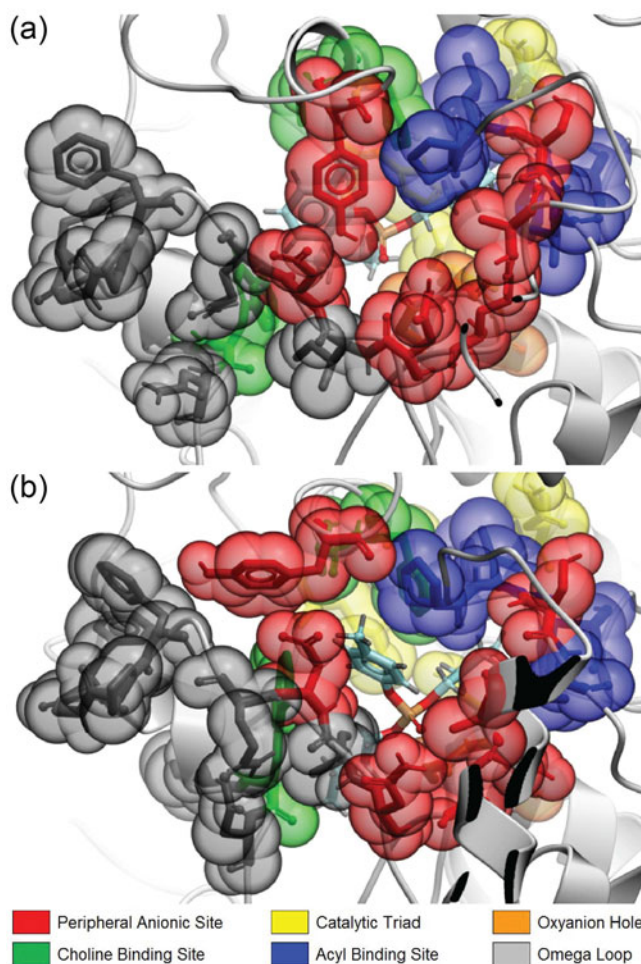


Figure 4. Magnified view of the BChE active site with (a) MET2 and (b) MET4 bound following the graphical conventions described in Figure 1. The structures shown are the average structures from the most stable binding modes observed.

when inhibitor size allows them to take positions adjacent to nearly any substituted functional group.

Visualizations of the primary binding modes of DIM4 and DIM5 shown in Figure 5(a,b), respectively, demonstrate the distinctly different orientations of these species within the active site gorge in tandem with relatively similar gorge structures. In Figure 5(a), the DIM4 aromatic group occupies the upper left quadrant of the pocket (from the perspective shown), and the phosphate $\text{P}=\text{O}$ oxygen points away from the active site toward the mouth of the gorge. In contrast, the orientation of the DIM5 phosphate group deep inside the active site, and the hydrogen bonding between phosphate group and CAT residues that results, fosters the interactions between the aromatic group and the numerous residues noted above.

3.4. Naphthyl-containing derivatives

Other than MET2, all mono-, di- and trimethylations of the DAP4 phenyl group discussed above showed significant impact on inhibitor binding strength. With this in mind, and the dominant role that the phenyl group aromaticity clearly plays in stabilizing inhibitor binding, a natural next step in

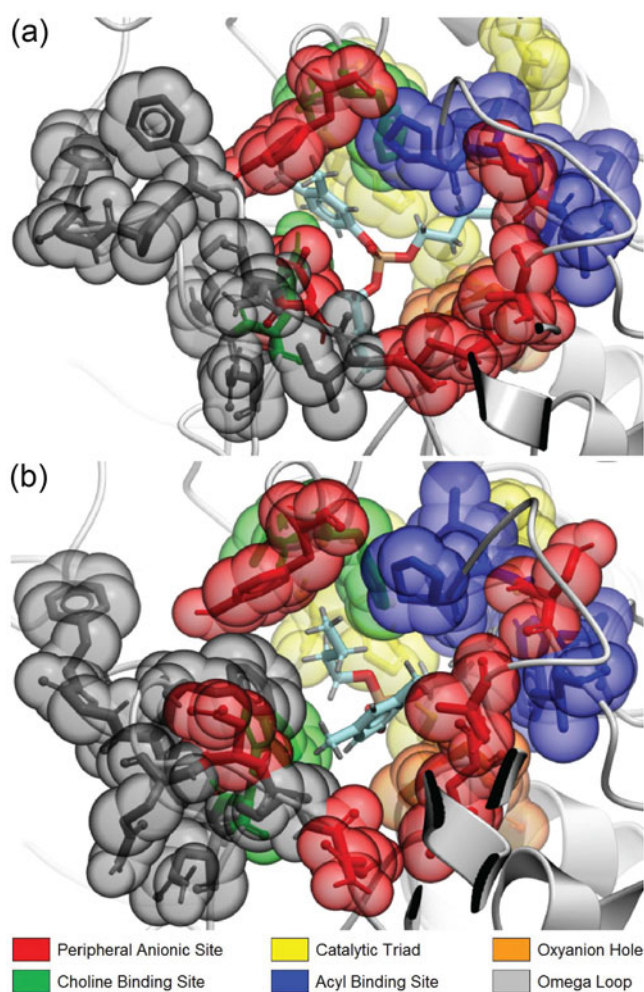


Figure 5. Magnified view of the BChE active site with (a) DIM4 and (b) DIM5 bound following the graphical conventions described in Figure 1. The structures shown are the average structures from the most stable binding modes observed.

Waals contact with GLN71 in the omega loop, which is not seen for DAP4. The sterically less-extended covalent connection of the naphthyl group to the phosphate in NAP1 thus favors these interactions between the NAP1 naphthyl group and omega loop residues, which are only minimally present in our NAP2 simulations. Indeed, an examination of omega loop positioning and motion after the initial equilibration period within our simulations confirms that NAP1 interactions with the OML hold that structure relatively in place, whereas the lack of NAP2 interactions with the OML allows for significantly larger deviation from the initial docked structure and more flexibility overall.

The visualizations of NAP1 and NAP2 in Figure 6(a,b), respectively, demonstrate this distinct difference in their omega loop positioning. While the NAP1 naphthyl appears to protrude farther toward the active site entrance, in relatively close proximity to omega loop residues, the analogous NAP2 naphthyl group favors a more internal orientation, yielding greater contact areas with active site residues in the PAS and CBS and leaving the OML residues largely without tether. The more extended structure resulting from the covalent linkage between the NAP2 naphthyl group and the phosphate also promotes consistent van der Waals contact

between inhibitor alkyl groups and ASN397, which was ubiquitous in our BChE–DAP4 simulations yet went unobserved in our BChE–NAP1 sampling. Overall, the seemingly minimal difference in positioning of the naphthyl group within the inhibitor has large-scale consequences in three-dimensional space that result in dramatically different enzyme active site structure and dynamics, with seemingly minor differences in enzyme–inhibitor interactions, yielding a 10-fold difference in binding affinity.

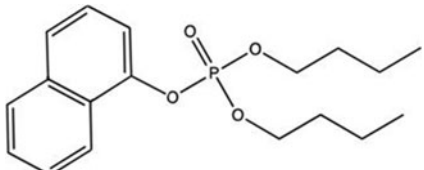
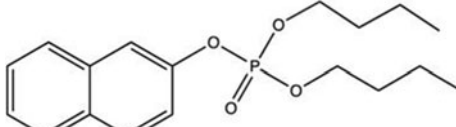
3.5. Choline-containing derivatives

As a final deviation from the basic DAP structure, a choline group, $-\text{CH}_2\text{CH}_2\text{N}^+(\text{CH}_3)_3$, was substituted in place of one of the two alkyl chains in an effort to mimic the chemistry of natural BChE substrates such as acetyl- and butyrylcholine. As this substitution results in stereoisomerism, the (*R*) and (*S*) forms were examined separately *in silico* alongside minor changes to the phenyl and alkyl substituents, as shown in Table 8. Although we have not yet published the experimental components of this study, racemic mixtures of several choline-containing DAP analogs were synthesized and assayed, as done in our previous report (Nakayama et al., 2017), leading to the K_i values presented in Table 8, and we are currently in the process of investigating the potential impact of the absolute stereochemistry on inhibitor binding strength.

As predicted by the docking scores for the CP4 and CB4 species in Table 8, the choline-containing inhibitors exhibit binding modes that depend directly on stereochemistry. The binding modes of (*S*)-enantiomers, shown in Table 9, largely reflect those of the reference DAP4: the OAH binds predominantly with the phosphate group, all residues in the ABS form non-polar van der Waals interactions with the alkyl group, the phenyl group forms π -stacking interactions with TYR332 in the PAS, and both the phosphate and phenyl groups interact with PHE339 in the CBS. The most prominent difference observed between our simulations of (*S*)-enantiomers and those of DAP4 was an increase in binding between the choline and phenyl groups with numerous amino acids in the surrounding APR, particularly residues GLU197, TRP430, MET437 and TYR440. The additional electrostatic and π -stacking interactions seen for (*S*)-enantiomers of the larger choline-containing inhibitors are thus expected to enhance the inhibition of their dialkyl analogs.

In contrast, (*R*)-enantiomers engage in qualitatively different binding behavior than that of DAP4, with contacts characterized by specific phosphate, phenyl and choline interactions within the active site gorge and the alkyl group solvated. The choline group supplants the previously seen phenyl ring position to interact with PAS and CBS residues and also engages in electrostatic interactions with GLU197 in the APR and both MET81 and GLN71 in the OML. This repositioning of the inhibitor relative to DAP4 binding allows (*R*)-enantiomers to maintain interactions between the phosphate group and GLY116 that were observed for DAP4 and replaces the similar phosphate–GLY117 interactions seen in DAP4 with phenyl–GLY117 contacts. The ubiquity of this contact

Table 6. Sampling, docking and assay results for the naphthyl-containing inhibitors.

Code	Nomenclature	Structure	Total time (ns)	Docking score	K_i (μM)
NAP1	dibutyl 1-naphthyl phosphate		290.9	-100.76 (± 0.87)	22 (± 2)
NAP2	dibutyl 2-naphthyl phosphate		479.7	-101.75 (± 1.02)	1.9 (± 0.4)

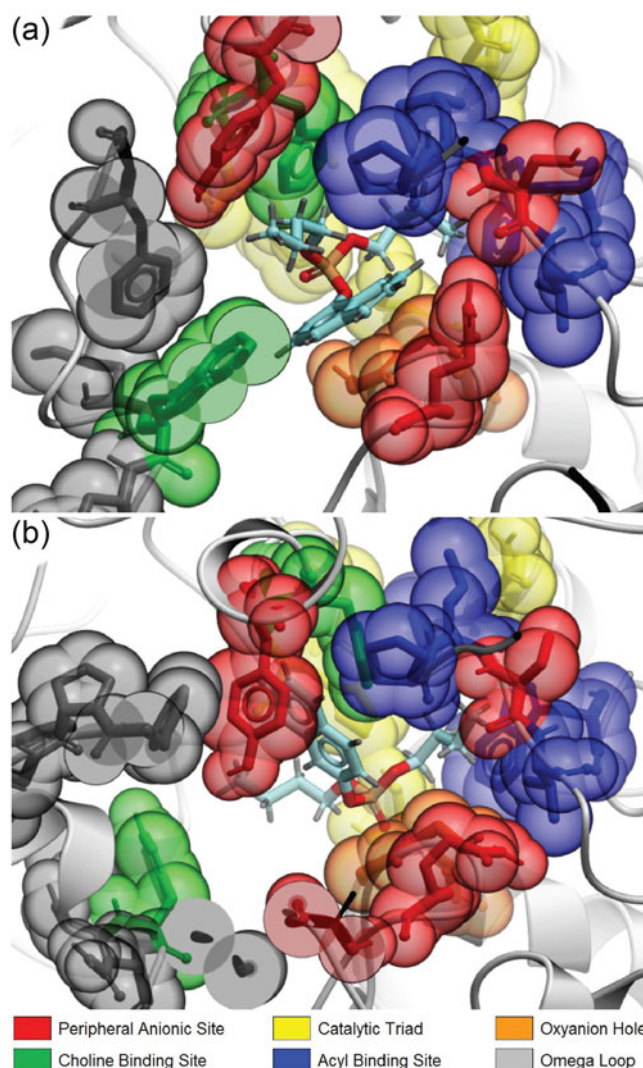


Figure 6. Magnified view of the BChE active site with (a) NAP1 and (b) NAP2 bound following the graphical conventions described in Figure 1. The structures shown are the average structures from the most stable binding modes observed.

between the phosphate (and now, phenyl) group with GLY116 and GLY117 emphasizes the importance of the oxyanion hole and the role it can play in stabilizing electron-dense regions of strong inhibitors.

In comparing the (*S*)- and the (*R*)-enantiomers (Figure 7), there is thus a discernible absence of choline and alkyl

contacts, respectively: that is, choline substitution of the pro-*S* butyl group with the choline moiety leaves interactions with the binding site largely unchanged, while choline substitution of the pro-*R* butyl group effectively replaces contacts between the alkyl group and the active site gorge with choline-gorge contacts. That electrostatics is a dominant intermolecular force cannot be underemphasized here, and the effective replacement of non-polar interactions with electrostatic interactions undoubtedly contributes significantly to the improved K_i value observed for the racemic CP4 mixture in comparison to the reference DAP4. It is therefore natural to accept the predictions of both docking calculations and MD simulations that predict the (*R*) form of CP4 and other choline-containing DAP analogs as the more inhibitory stereoisomers, which largely determine the degree to which these choline-containing species outperform their DAP analogs. Initial synthetic and assay efforts to evaluate CP4r and CP4s inhibition constants suggest that the (*R*) stereoisomer is indeed the stronger inhibitor (to be published).

3.6. The omega loop and TRP82

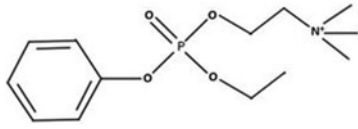
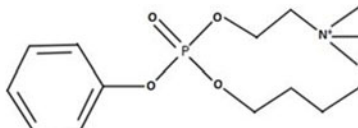
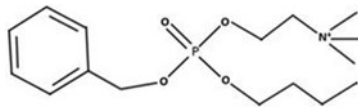
It is well established that the omega loop of AChE undergoes conformational changes in the presence of substrate and some reversible inhibitors (Shi, Radic, & Taylor, 2002) and also exhibits a gating behavior that imparts acetylcholine specificity by physically blocking substrate access to the active site for larger substrates (Stank, Kokh, Fuller, & Wade, 2016; Zhou, Wlodek, & McCammon, 1998). In contrast, the OML region of BChE in our simulations does not exhibit this gating behavior in the absence or presence of inhibitors. Rather, we observe conformational changes including (i) an 'open' state in which the OML is fully solvent-exposed and allows access of small molecules to the active site gorge (Figure 1(a)), alongside (ii) a structural preference of the active site gorge for 'closed' configurations via two possible mechanisms. The first involves the closing of the OML into the mouth of the active site gorge, resulting in 'capping' of the gorge (Figure 8(a)), in which hydrophobic residues within the OML and the ABS are in contact. In the second, the peripheral anionic site and acyl binding site come together to 'pinch off' access to the gorge (Figure 4(a)), with MET2

Table 7. Contacts observed in the most populated binding modes of the naphthyl inhibitors.

Inh. & Mode	ASN68	ASP70	GLN119	ALA277	SER287	TYR332	SER198	GLU325	HIS438	GLY116	GLY117	ALA199	TRP82	ALA328	PHE329	TRP231	PRO285	LEU286	VAL288	PHE398	ILE69	GLN71	PHE73	PRO74	GLY75	PHE76	MET81	ASN83	SER79	TYR114	GLY115	PHE118	THR120	TYR128	GLU197	ASN397	TRP490	MET437	GLY439	TYR440	ILE442												
NAP1	PAS		CAT					OAH			CBS				ABS				OML										Additional Protein Residues (APR)																								
0	Nap		Nap		Alk		Alk		PO ₄	Nap	PO ₄		Nap	PO ₄	Alk	Nap	Alk	Alk	Alk	Alk																																	
1		Nap			Alk	Nap	Alk		PO ₄	PO ₄	PO ₄		Nap	PO ₄	Alk	Nap	Alk	Alk	Alk	Alk																																	
2			Nap		Alk	Nap	PO ₄		PO ₄	Nap	PO ₄		Nap	PO ₄	Alk	Nap	Alk	Alk	Alk	Alk																																	
3			Nap		Alk	Nap	Alk		Alk	PO ₄	PO ₄		Nap	PO ₄	Alk	Nap	Alk	Alk	Alk	Alk																																	
4	PO ₄		PO ₄		Alk		Alk		Alk	Alk	PO ₄		Nap	PO ₄	Alk	Nap	Alk	Alk	Alk	Alk																																	
NAP2	PAS		CAT					OAH			CBS				ABS				OML										Additional Protein Residues (APR)																								
0		Alk	Alk	Alk	Nap	PO ₄	PO ₄	PO ₄	PO ₄	PO ₄	PO ₄		Nap	Nap	Nap	Alk	Nap	Alk	Alk	Alk																																	
1	Nap		Nap		Alk		Alk		PO ₄	PO ₄	PO ₄		Nap	PO ₄	Alk	Nap	Alk	Alk	Alk	Alk																																	
2			Nap		Alk	Nap	PO ₄		PO ₄	Nap	PO ₄		Nap	PO ₄	Alk	Nap	Alk	Alk	Alk	Alk																																	
3	Nap		Nap		Alk	Nap	Alk		Alk	PO ₄	PO ₄		Nap	PO ₄	Alk	Nap	Alk	Alk	Alk	Alk																																	
4			Nap		Alk	Nap	Alk		Alk	PO ₄	PO ₄		Nap	PO ₄	Alk	Nap	Alk	Alk	Alk	Alk																																	

Legend: ■ Electrostatic ■ Hydrogen Bonding ■ Cation- π ■ π -stacking ■ van der Waals ■ Non-polar Backbone

Table 8. Sampling, docking and assay results for the choline-containing inhibitors.

Code	Nomenclature	Structure	Total time (ns)	Docking score	K_i (μ M)
CP2r	ethyl choline phenyl phosphate		259.8	-80.04 (\pm 2.22)	30.0 (\pm 1)
CP2s			259.4	-79.25 (\pm 2.34)	
CP4r	butyl choline phenyl phosphate		220.3	-91.72 (\pm 0.48)	10.5 (\pm 0.27)
CP4s			214.1	-89.99 (\pm 0.74)	
CB4r	butyl choline benzyl phosphate		259.4	-103.34 (\pm 1.51)	N/A
CB4s			259.8	-100.92 (\pm 1.10)	

bound), and the link between the PAS and the OML results in the OML being pulled into a partially closed position.

These two closed conformations (capped and pinched) were observed frequently for non-choline-containing inhibitors, some choline-containing (*S*)-enantiomers and BChE *sans* inhibitor. That these conformations are observed in the absence of inhibitors establishes that they are natural states of the protein and, more specifically, the active site. While the limited sampling reported herein does not allow us to approximate the statistical weights of these closed states or the open state represented by Figure 1(a), that these closed conformations appear to dominate our sampling suggests that OML position and dynamics play an important role in the inhibition process, and one might then surmise that inhibitors of proper size, geometry and/or chemistry might be more omega loop compatible, or complementary, than other inhibitors.

Indeed, the choline-containing (*R*)-enantiomers appear to achieve such complementarity with the OML and the adjacent choline-binding site. The binding of (*R*)-enantiomers, as discussed above, includes consistent choline cation- π interactions with TRP82. The result of this interaction and the binding orientation that fosters it, particularly for the more strongly binding CP4r and CB4r species, is the observation of a fourth omega loop state in which the OML is mechanically leveraged into a wide open and rigid conformation (Figure 8(b)) that exposes the active site gorge to a greater extent than the natural 'open' state seen in Figure 1(a). A plot of

the change in root-mean-squared fluctuation per residue (Δ RMSF) is shown in Figure 8(c). As shown there, the flexibility of omega loop residues is greatly reduced when CP4r or CB4r is bound. This, of course, raises the question: *what is the purpose of such mechanical leveraging of the omega loop into an open position that fully exposes the active site gorge?*

We speculate that this mechanism acts to counter the observation that closed conformations of the gorge and omega loop are thermodynamically preferred for BChE. That is, trapping of the products of catalysis by closed-gorge conformations, via capping or pinching, would not provide those products to the local area in which they are needed and would instead temporarily lock the enzyme in a non-functional state. However, if natural substrates such as butyrylcholine exhibit this mechanical leveraging of the OML into an open position, thus exposing the active site gorge, increased rates of product emission and substrate arrival would be expected, thereby contributing to BChE efficiency and providing product species to the local environment.

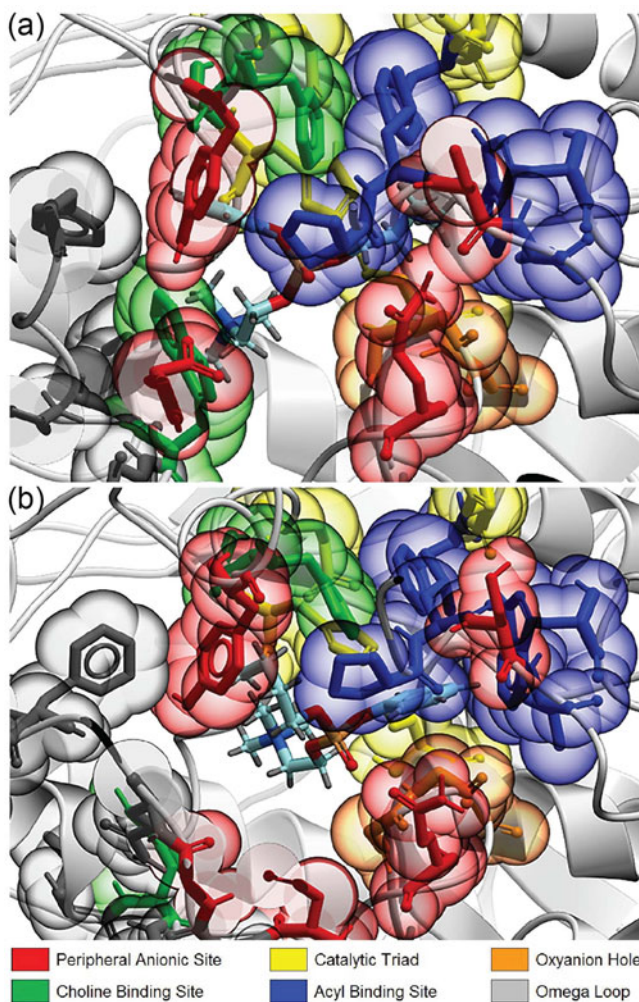
4. Conclusion

The clustering of structures from all-atom MD simulations allowed for characterization of distinct BChE-inhibitor binding modes, which are intricate and fluid three-dimensional engagements that are concisely summarized via contact tables. Examination of these contact tables revealed several motifs of particular interest. First, the enlargement of a

Table 9. Contacts observed in the most populated binding modes of the choline-containing inhibitors.

Inh. & Mode	ASN68	ASP70	GLN119	ALA277	SER287	TYR332	SER198	GLU25	HIS438	GLY116	GLY117	ALA199	TRP92	ALA228	PHE229	TRP231	PRO265	LEU266	VAL268	PHE398	ILE69	GLN71	PHE73	PRO74	GLY75	PHE76	MET81	ASN83	SER79	TYR114	GLY115	PHE118	THR120	TYR128	GLU197	ASN97	TRP400	MET437	GLY439	TYR440	ILE442		
CP2r	PAS			CAT			OAH			CBS			ABS			OML												Additional Protein Residues (APR)															
0							Ch		Ch	PO ₄	Ph	Ch			Ph	Ph	Ph	Ph	Ph	Ph												Ch	Ch			Ch						Ch	Ch
1							Ch	Ch	Ch	PO ₄	Ph	PO ₄	Ch			Ph	Ph	Ph	Ph	Ph												PO ₄	Ch			Ch						Ch	Ch
2			PO ₄		Ph	Ch	Ch	Ch	Ch	PO ₄	Ph	Ch	Ch	Ch	PO ₄	Ph	Ph	Ph	Ph	Ph	Ch										Ch	Ch	PO ₄		Ch						Ch	PO ₄	Ch
CP2s	PAS			CAT			OAH			CBS			ABS			OML												Additional Protein Residues (APR)															
0							Ph	PO ₄		PO ₄	PO ₄	PO ₄			Ph	Ph	Alk	PO ₄	Alk	Alk													Ph		PO ₄							Ch	
1							Ph	PO ₄		PO ₄	PO ₄	PO ₄			PO ₄	Ph	Alk	PO ₄	Alk	Alk												Ph		PO ₄								Ch	
2							Ph	PO ₄		PO ₄	PO ₄	PO ₄			PO ₄	Alk	Alk	Alk	Alk	Alk											Ph		PO ₄									Ch	
CP4r	PAS			CAT			OAH			CBS			ABS			OML												Additional Protein Residues (APR)															
0							Ch		Ch	PO ₄	Ph	Ph	Ch			Ph	Ph	Ph	Ph	Ph	Ph											Ch		PO ₄	Ch	Ch						Ch	Ch
1	Ch	Ch	PO ₄				Ch	Ch	Ch	PO ₄	Ph	Ch	Alk	Ph	Ph	Ph	Ph	Ph	Ph	Ph	Ch											Ch		PO ₄	Ch	Ch		Ch				Ch	Ch
2	Ch	Ch	Ch				Ch	Ch	Ch	PO ₄	Ph	Ch			Ph	Ph	Ph	Ph	Ph	Ph	Ch										Ch		PO ₄	Ch	Ch	Ch	Ch	Ch	Ch	Ch	Ch	Ch	
CP4s	PAS			CAT			OAH			CBS			ABS			OML												Additional Protein Residues (APR)															
0							Ph	Alk		Ph	PO ₄	Alk	Alk	Ph	Ph	Ph	Alk	PO ₄	Alk	Alk	Alk													PO ₄	Alk			Ph				Ph	
1							Ph	Alk		Ph	PO ₄	Alk	Alk	Ph	Ph	Ph	Alk	PO ₄	Alk	Alk	Alk													PO ₄	Alk			Ph				Ph	
2							Ph	Alk		Ph	PO ₄	Alk	Alk	Ph	Ph	Ph	Alk	PO ₄	Alk	Alk	Alk													PO ₄	Alk			Ph	Ph	Ch	Ph		
CB4r	PAS			CAT			OAH			CBS			ABS			OML												Additional Protein Residues (APR)															
0			PO ₄				Ph		Ph	PO ₄	Ph	Ch			Ph	Ph	Ph	Ph	Ph	Ph	Ch											Ch		PO ₄	Ch	Ch	Ch	Ch	Ch	Ch	Ch	Ch	
1			PO ₄				Ch	Ph		Ch	PO ₄	Ph	Ch			Ph	Ph	Ph	Ph	Ph	Ch											Ch		PO ₄	Ch	Ch	Ch	Ch	Ch	Ch	Ch	Ch	
2			PO ₄				Ch	Ph		Ch	PO ₄	Ph	Ch	Ch	Ch	Ph	Ph	Ph	Ph	Ph	Ch	Ch										Ch		PO ₄	Ch	Ch	Ch	Ch	Ch	Ch	Ch	Ch	
CB4s	PAS			CAT			OAH			CBS			ABS			OML												Additional Protein Residues (APR)															
0							Ph	Alk		PO ₄	PO ₄	Alk	Alk	Ph	Ph	Ph	PO ₄	Alk	Alk	Alk	Alk														Ph			Ph			Ch	Ph	
1							Ph	Alk		Ph	PO ₄	Alk	Alk	Ph	Ph	Ph	PO ₄	Alk	Alk	Alk	Alk														PO ₄	Alk	Ph		PO ₄	Ph	Ph	Ch	Ch
2							Ph	PO ₄		Alk	PO ₄	PO ₄	PO ₄	Ph	Ph	Ph	PO ₄	Alk	Alk	Alk	Alk														PO ₄	Alk	Ph		PO ₄	Ph	Ph	Ch	Ch

■ Electrostatic
 ■ Hydrogen Bonding
 ■ Cation- π
 ■ π -stacking
 ■ van der Waals
 ■ Non-polar
 ■ Backbone


Figure 7. Magnified view of the BChE active site with (a) CP4r and (b) CP4s bound following the graphical conventions described in Figure 1. The structures shown are the average structures from the most stable binding modes observed.

specific functional group by substitution of a chemically similar species, such as the replacement of a phenyl ring with a naphthyl group, allows the derivative species to maintain many of the originally observed contacts while potentially increasing the area of contact between that group and the active site gorge. Second, contacts formed by oxyanion hole residues GLY116 and GLY117 are ubiquitous, appearing in nearly every binding mode for every inhibitor studied and most often involve the inhibitor phosphate group, which replaces the anionic transition state that is inherent to catalysis. Future design of cholinesterase inhibitors might then begin by assuming significant phosphate–OAH contact and constructing outwardly from there. Third, and most surprising, is the clear and significant dependence of binding strength on stereochemistry: (*S*)-enantiomers studied herein maintained the binding behavior of the base structure, DAP4, whereas (*R*)-enantiomers consistently adopted different binding poses that employed electrostatic interactions to strengthen BChE–inhibitor contact. Lastly, splaying of the active site gorge upon the formation of choline–CBS contact effectively counteracts the thermodynamic favoring of closed-gorge BChE conformations, which we attribute to molecular evolution toward more efficient catalysis.

More generally, this work presents a method to ascertain and graphically display the observed binding modes of a simulated protein–inhibitor complex. As raw computational power, algorithmic sophistication and large-scale resources now enable massive sampling (Borhani & Shaw, 2012; De Vivo, Masetti, Bottegoni, & Cavalli, 2016; Sorin et al., 2017), it is important to regularly assess both our computational models and the predictions they make. With that in mind, and given the success of this initial proof-of-concept effort that employed limited computational sampling, we are currently simulating BChE–inhibitor complexes on a much larger scale with the aim of accumulating statistically relevant (and, therefore, thermodynamically relevant) sampling of binding

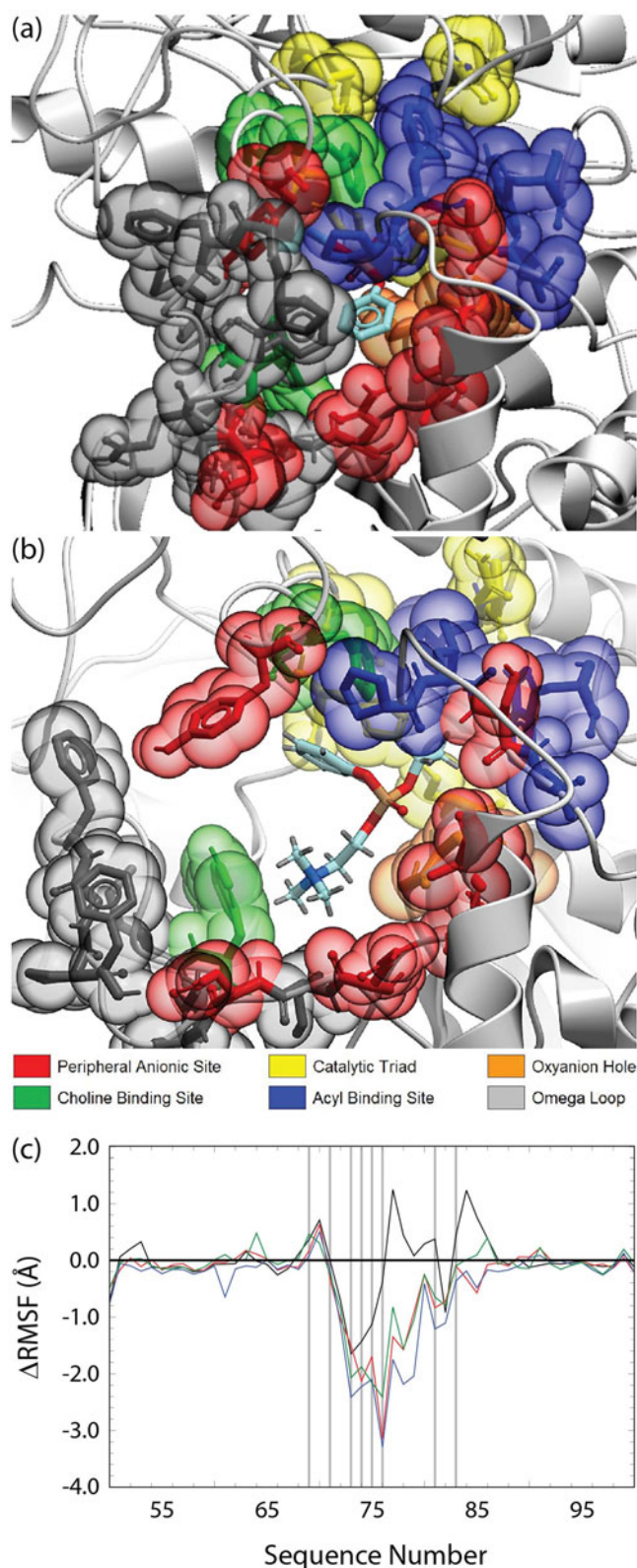


Figure 8. Magnified view of the BChE active site, following the graphical conventions described in Figure 1, with (a) DAP4 bound inside a capped gorge structure and (b) CP2r bound inside a wide open gorge structure. (c) Changes in atomic root-mean-squared fluctuations of residues in and around the omega loop region of BChE, as compared to the enzyme *sans* inhibitor, are shown for the enzyme in complex with the reference inhibitor DAP4 (black), CP2r (green), CP4r (blue) and CB4r (red). Omega loop residues not assigned to adjacent active site regions are denoted by vertical lines.

modes and omega loop positions available to these complexes and to the protein *sans* inhibitor. We are also exploring the use of more sophisticated descriptors of inhibitor-active site contacts, with the goal of systematically identifying and discriminating between similar but non-identical binding modes in a fully reproducible and non-heuristic manner. It is expected that by significantly enhancing both the per-complex sampling and the quality of the clustering vector that describes protein-inhibitor interactions will allow for the most accurate predictions of statistical weights and relative free energies of all sampled binding modes for a given complex.

Acknowledgements

The content is solely the responsibility of the authors and does not necessarily represent the official views of the National Institutes of Health. WA acknowledges support from the Margaret Heeb and Philip Ord Johnson Scholarship programs. PB was supported by a CSULB Summer Research Assistantship and a Robert B. Henderson Memorial Scholarship. AC would like to thank Boeing and the CSULB College of Engineering for scholarship support.

Funding

Research reported in this publication was supported, in part, by the NIH National Institute of General Medical Sciences [award numbers T34GM008074 and R25GM071638], as well as the NSF MRI program [CHE-1337559].

References

- Abagyan, R. A., Totrov, M. M., & Kuznetsov, D. A. (1994). ICM: A new method for protein modeling and design: Applications to docking and structure prediction from the distorted native conformation. *Journal of Computational Chemistry*, *15*(5), 488–506. doi:10.1002/jcc.540150503
- Akincioglu, A., Kocaman, E., Akincioglu, H., Salmas, R. E., Durdagi, S., Gulcin, I., ... Goksu, S. (2017). The synthesis of novel sulfamides derived from β -benzylphenethylamines as acetylcholinesterase, butyrylcholinesterase and carbonic anhydrase enzymes inhibitors. *Bioorganic Chemistry*, *74*, 238–250. doi:10.1016/j.bioorg.2017.08.012
- Allderdice, P. W., Gardner, H. A. R., Galutira, D., Lockridge, O., Ladu, B. N., & McAlpine, P. J. (1991). The cloned butyrylcholinesterase (BChE) gene maps to a single chromosome site, 3q26. *Genomics*, *11*(2), 452–454.
- An, J., Totrov, M., Abagyan R. (2005). Pocketome via comprehensive identification and classification of ligand binding envelopes. *Molecular & Cellular Proteomics*, *4*(6), 752–761. doi:10.1074/mcp.M400159-MCP200
- Berendsen, H. J. C., Postma, J. P. M., van Gunsteren, W. F., DiNola, A., & Haak, J. R. (1984). Molecular dynamics with coupling to an external bath. *Journal of Chemical Physics*, *81*(8), 3684–3690. doi:10.1063/1.448118
- Biberoglu, K., Tacal, O., & Akbulut, H. (2011). The role of Phe329 in binding of cationic triarylmethane dyes to human butyrylcholinesterase. *Archives of Biochemistry and Biophysics*, *511*(1–2), 64–68. doi:10.1016/j.abb.2011.04.007
- Biovia, D. S. (2007). *Discovery Studio Modeling Environment, Version 2.5. BIOVIA Workbook, Release 2017; BIOVIA Pipeline Pilot, Release 2017*. San Diego, CA: Dassault Systèmes.
- Borhani, D. W., & Shaw, D. E. (2012). The future of molecular dynamics simulations in drug discovery. *Journal of Computer-Aided Molecular Design*, *26*(1), 15–26. doi:10.1007/s10822-011-9517-y

- Bussi, G., Donadio, D., & Parrinello, M. (2007). Canonical sampling through velocity rescaling. *Journal of Chemical Physics*, 126(1), 014101. doi:10.1063/1.2408420
- Cavallaro, V., Moglie, Y. F., Murray, A. P., & Radivoy, G. E. (2018). Alkynyl and β -ketophosphonates: Selective and potent butyrylcholinesterase inhibitors. *Bioorganic Chemistry*, 77, 420–428. doi:10.1016/j.bioorg.2018.01.030
- Chatonnet, A., & Lockridge, O. (1989). Comparison of butyrylcholinesterase and acetylcholinesterase. *The Biochemical Journal*, 260(3), 625–634.
- Chiou, S. Y., Huang, C. F., Hwang, M. T., & Lin, G. (2009). Comparison of active sites of butyrylcholinesterase and acetylcholinesterase based on inhibition by geometric isomers of benzene-di-*N*-substituted carbamates. *Journal of Biochemical and Molecular Toxicology*, 23(5), 303–308. doi:10.1002/jbt.20286
- Darvesh, S., Hopkins, D. A., & Geula, C. (2003). Neurobiology of butyrylcholinesterase. *Nature Reviews. Neuroscience*, 4(2), 131–138. doi:10.1038/nrn1035
- De Vivo, M., Masetti, M., Bottegoni, G., & Cavalli, A. (2016). Role of molecular dynamics and related methods in drug discovery. *Journal of Medicinal Chemistry*, 59(9), 4035–4061. doi:10.1021/acs.jmedchem.5b01684
- Dighe, S. N., Deora, G. S., De la Mora, E., Nachon, F., Chan, S., Parat, M.-O., ... Ross, B. P. (2016). Discovery and structure–activity relationships of a highly selective butyrylcholinesterase inhibitor by structure-based virtual screening. *Journal of Medicinal Chemistry*, 59(16), 7683–7689. doi:10.1021/acs.jmedchem.6b00356
- Dong, M. X., Xu, X. M., Hu, L., Liu, Y., Huang, Y. J., & Wei, Y. D. (2017). Serum butyrylcholinesterase activity: A biomarker for Parkinson's disease and related dementia. *BioMed Research International*, 2017, 1. doi:10.1155/2017/1524107
- Duan, Y., Wu, C., Chowdhury, S., Lee, M. C., Xiong, G., Zhang, W., ... Kollman, P. (2003). A point-charge force field for molecular mechanics simulations of proteins based on condensed-phase quantum mechanical calculations. *Journal of Computational Chemistry*, 24(16), 1999–2012. doi:10.1002/jcc.10349
- Ellingson, B. A., Geballe, M. T., Wlodek, S., Bayly, C. I., Skillman, A. G., & Nicholls, A. (2014). Efficient calculation of SAMPL₄ hydration free energies using OMEGA, SZYBKI, QUACPAC, and Zap TK. *Journal of Computer-Aided Molecular Design*, 28(3), 289–298. doi:10.1007/s10822-014-9720-8
- Farlow, M. R., & Cyrus, P. A. (2000). Metrifonate therapy in Alzheimer's disease: A pooled analysis of four randomized, double-blind, placebo-controlled trials. *Dementia and Geriatric Cognitive Disorders*, 11(4), 202–211.
- Fetrow, J. S. (1995). Omega loops: Nonregular secondary structures significant in protein function and stability. *Faseb Journal : Official Publication of the Federation of American Societies for Experimental Biology*, 9(9), 708–717.
- Fukuto, T. R., & Metcalf, R. L. (1956). Pesticidal activity and structure, structure and insecticidal activity of some diethyl substituted phenyl phosphates. *Journal of Agricultural and Food Chemistry*, 4(11), 930–935. doi:10.1021/jf60069a001
- Giacobini, E. (2001). Selective inhibitors of butyrylcholinesterase: A valid alternative for therapy of Alzheimer's disease? *Drugs & Aging*, 18(12), 891–898. doi:10.2165/00002512-200118120-00001
- Giacobini, E. (2004). Cholinesterase inhibitors: New roles and therapeutic alternatives. *Pharmacological Research*, 50(4), 433–440. doi:10.1016/j.phrs.2003.11.017
- Greig, N. H., Utsuki, T., Ingram, D. K., Wang, Y., Pepeu, G., Scali, C., ... Lahiri, D. K. (2005). Selective butyrylcholinesterase inhibition elevates brain acetylcholine, augments learning and lowers Alzheimer β -amyloid peptide in rodent. *Proceedings of the National Academy of Sciences of the United States of America*, 102(47), 17213–17218. doi:10.1073/pnas.0508575102
- Guex, N., & Peitsch, M. C. (1997). SWISS-MODEL and the Swiss-PdbViewer: An environment for comparative protein modeling. *Electrophoresis*, 18(15), 2714–2723. doi:10.1002/elps.1150181505
- Hess, B., Bekker, H., Berendsen, H. J. C., & Fraaije, J. G. E. M. (1997). LINCS: A linear constraint solver for molecular simulations. *Journal of Computational Chemistry*, 18(12), 1463–1472. doi:10.1002/(SICI)1096-987X(199709)18:12<1463::AID-JCC4>3.0.CO;2-H
- Hong, S.-B., & Raushel, F. M. (1999). Stereochemical constraints on the substrate specificity of phosphotriesterase. *Biochemistry*, 38(4), 1159–1165. doi:10.1021/bi982204m
- Jakalian, A., Bush, B. L., Jack, D. B., & Bayly, C. I. (2000). Fast, efficient generation of high-quality atomic charges. AM1-BCC model: I. Method. *Journal of Computational Chemistry*, 21(2), 132–146. doi:10.1002/(SICI)1096-987X(20000130)21:2<132::AID-JCC5>3.3.CO;2-G
- Jakalian, A., Jack, D. B., & Bayly, C. I. (2002). Fast, efficient generation of high-quality atomic charges. AM1-BCC model: II. Parameterization and validation. *Journal of Computational Chemistry*, 23(16), 1623–1641. doi:10.1002/jcc.10128
- Kamal, M. A., Qu, X., Yu, Q.-S., Tweedie, D., Holloway, H. W., Li, Y., ... Greig, N. H. (2008). Tetrahydrofurobenzofuran cymserine, a potent butyrylcholinesterase inhibitor and experimental Alzheimer drug candidate, enzyme kinetic analysis. *Journal of Neural Transmission*, 115(6), 889–898. doi:10.1007/s00702-008-0022-y
- Law, K.-S., Acey, R. A., Smith, C. R., Benton, D. A., Soroushian, S., Eckenrod, B., ... Nakayama, K. (2007). Dialkyl phenyl phosphates as novel selective inhibitors of butyrylcholinesterase. *Biochemical and Biophysical Research Communications*, 355(2), 371–378. doi:10.1016/j.bbrc.2007.01.186
- Mahoney, M. W., & Jorgensen, W. L. (2000). A five-site model for liquid water and the reproduction of the density anomaly by rigid, nonpolarizable potential functions. *Journal of Chemical Physics*, 112(20), 8910–8922. doi:10.1063/1.481505
- Masson, P., Froment, M. T., Bartels, C. F., & Lockridge, O. (1996). Asp70 in the peripheral anionic site of human butyrylcholinesterase. *European Journal of Biochemistry*, 235(1–2), 36–48. doi:10.1111/j.1432-1033.1996.00036.x
- Masson, P., Legrand, P., Bartels, C. F., Froment, M. T., Schopfer, L. M., & Lockridge, O. (1997). Role of aspartate 70 and tryptophan 82 in binding of succinylthiocholine to human butyrylcholinesterase. *Biochemistry*, 36(8), 2266–2277. doi:10.1021/bi962484a
- Masson, P., Xie, W., Froment, M. T., & Lockridge, O. (2001). Effects of mutations of active site residues and amino acids interacting with the Omega loop on substrate activation of butyrylcholinesterase. *Biochimica et Biophysica Acta*, 1544(1–2), 166–176. doi:10.1016/S0167-4838(00)00217-X
- Mesulam, M. M., Guillozet, A., Shaw, P., Levey, A., Duysen, E. G., & Lockridge, O. (2002). Acetylcholinesterase knockouts establish central cholinergic pathways and can use butyrylcholinesterase to hydrolyze acetylcholine. *Neuroscience*, 110(4), 627–639. doi:10.1016/S0306-4522(01)00613-3
- Moretto, A. (1998). Experimental and clinical toxicology of anticholinesterase agents. *Toxicology Letters*, 102, 509–513. doi:10.1016/S0378-4274(98)00245-8
- Nakayama, K., Schwans, J. P., Sorin, E. J., Tran, T., Gonzalez, J., Arteaga, E., ... Alvarado, W. (2017). Synthesis, biochemical evaluation, and molecular modeling studies of aryl and arylalkyl di-*n*-butyl phosphates, effective butyrylcholinesterase inhibitors. *Bioorganic & Medicinal Chemistry*, 25(12), 3171–3181. doi:10.1016/j.bmc.2017.04.002
- Nicolet, Y., Lockridge, O., Masson, P., Fontecilla-Camps, J. C., & Nachon, F. (2003). Crystal structure of human butyrylcholinesterase and of its complexes with substrate and products. *Journal of Biological Chemistry*, 278(42), 41141–41147. doi:10.1074/jbc.M210241200
- Pezzementi, L., Nachon, F., & Chatonnet, A. (2011). Evolution of acetylcholinesterase and butyrylcholinesterase in the vertebrates: An atypical butyrylcholinesterase from the *Medaka Oryzias latipes*. *PLoS ONE*, 6(2), e17396. doi:10.1371/journal.pone.0017396
- Pronk, S., Páll, S., Schulz, R., Larsson, P., Bjelkmar, P., Apostolov, R., ... Lindahl, E. (2013). GROMACS 4.5: A high-throughput and highly parallel open source molecular simulation toolkit. *Bioinformatics*, 29(7), 845–854. doi:10.1093/bioinformatics/btt055
- Rahimi, Z., Ahmadi, R., Vaisi-Raygani, A., Rahimi, Z., Bahreghmand, F., & Parsian, A. (2013). Butyrylcholinesterase (BChE) activity is associated with the risk of preeclampsia: Influence on lipid and lipoprotein metabolism and oxidative stress. *Journal of Maternal-Fetal & Neonatal Medicine*, 26(16), 1590–1594. doi:10.3109/14767058.2013.795534

- Senol, F. S., Ślusarczyk, S., Matkowski, A., Pérez-Garrido, A., Girón-Rodríguez, F., Cerón-Carrasco, J. P., ... Orhan, I. E. (2017). Selective *in vitro* and *in silico* butyrylcholinesterase inhibitory activity of diterpenes and rosmarinic acid isolated from *Perovskia atriplicifolia* Benth. and *Salvia glutinosa* L. *Phytochemistry*, 133, 33–44. doi:10.1016/j.phytochem.2016.10.012
- Shao, J., Tanner, S. W., Thompson, N., & Cheatham, T. E. (2007). Clustering molecular dynamics trajectories: 1. Characterizing the performance of different clustering algorithms. *Journal of Chemical Theory and Computation*, 3(6), 2312–2334. doi:10.1021/ct700119m
- Shi, J., Radic, Z., & Taylor, P. (2002). Inhibitors of different structure induce distinguishing conformations in the omega loop, Cys69–Cys96, of mouse acetylcholinesterase. *Journal of Biological Chemistry*, 277(45), 43301–43308. doi:10.1074/jbc.M204391200
- Sirin, G., & Zhang, Y. (2014). How is acetylcholinesterase phosphorylated by Soman? An *ab initio* QM/MM molecular dynamics study. *The Journal of Physical Chemistry A*, 118(39), 9132–9139. doi:10.1021/jp502712d
- Sorin, E. J., Alvarado, W., Cao, S., Radcliffe, A., La, P., & An, Y. (2017). Ensemble molecular dynamics of a protein–ligand complex: Residual inhibitor entropy enhances drug potency in butyrylcholinesterase. *Bioenergetics*, 6(1). doi:10.4172/2167-7662.1000145.
- Sorin, E. J., & Pande, V. S. (2005). Exploring the helix-coil transition via all-atom equilibrium ensemble simulations. *Biophysical Journal*, 88(4), 2472–2493. doi:10.1529/biophysj.104.051938
- Stank, A., Kokh, D. B., Fuller, J. C., & Wade, R. C. (2016). Protein binding pocket dynamics. *Accounts of Chemical Research*, 49(5), 809–815. doi:10.1021/acs.accounts.5b00516
- Wandhammer, M., Carletti, E., Van der Schans, M., Gillon, E., Nicolet, Y., Masson, P., ... Nachon, F. (2011). Structural study of the complex stereoselectivity of human butyrylcholinesterase for the neurotoxic V-agents. *Journal of Biological Chemistry*, 286(19), 16783–16789. doi:10.1074/jbc.M110.209569
- Wang, J., Wolf, R. M., Caldwell, J. W., Kollman, P. A., & Case, D. A. (2004). Development and testing of a general AMBER force field. *Journal of Computational Chemistry*, 25(9), 1157–1174. doi:10.1002/jcc.20035
- Warshel, A., Naray-Szabo, G., Sussman, F., & Hwang, J. K. (1989). How do serine proteases really work? *Biochemistry*, 28(9), 3629–3637.
- Yu, Y.-F., Huang, Y.-D., Zhang, C., Wu, X.-N., Zhou, Q., Wu, D., ... Luo, H.-B. (2017). Discovery of novel pyrazolopyrimidinone derivatives as phosphodiesterase 9A inhibitors capable of inhibiting butyrylcholinesterase for treatment of Alzheimer's disease. *ACS Chemical Neuroscience*, 8(11), 2522–2534. doi:10.1021/acschemneuro.7b00268
- Zhan, C.-G., & Gao, D. (2005). Catalytic mechanism and energy barriers for butyrylcholinesterase-catalyzed hydrolysis of cocaine. *Biophysical Journal*, 89(6), 3863–3872. doi:10.1529/biophysj.105.070276
- Zhou, H.-X., Wlodek, S. T., & McCammon, J. A. (1998). Conformation gating as a mechanism for enzyme specificity. *Proceedings of the National Academy of Sciences*, 95(16), 9280–9283. doi:10.1073/pnas.95.16.9280